Three Dimensional Extended Boundary Node Method to Potential Problem

Taku ITOH, Ayumu SAITOH[1)], Atsushi KAMITANI[2)] and Hiroaki NAKAMURA[3)]

Faculty of Science and Technology, Seikei University, Musashino, Tokyo 180-8633, Japan
[1)]*Graduate School of Engineering, University of Hyogo, Himeji, Hyogo 671-2280, Japan*
[2)]*Graduate School of Science and Engineering, Yamagata University, Yonezawa, Yamagata 992-8510, Japan*
[3)]*National Institute for Fusion Science, Toki, Gifu 509-5292, Japan*

(Received 8 December 2009 / Accepted 25 February 2010)

A three-dimensional boundary-node method without any integration cells has been formulated. In the proposed method, an implicit surface is assumed as a surface boundary, and the 3D local coordinates are used to evaluate surface integrals. Numerical experiments illustrate that although the computational costs of the proposed method are larger than those of the boundary element method (BEM), the proposed method enables the evaluation of surface integrals without any integration cells. In addition, the accuracy of the proposed method is almost the same as that of the BEM for the Laplace problem.

Keywords: boundary node method, boundary element method, integration cell, implicit function, 3D problem

DOI: 10.1585/pfr.5.S2111

1. Introduction

Potential problems often appear in various engineering fields such as the nuclear fusion. The boundary-element method (BEM) has been applied to these problems and has produced many excellent results; however, a boundary surface must be divided into a set of boundary elements before the BEM is applied to the problems.

Alternatively, Chati *et al.* have proposed the boundary-node method (BNM) [1] as a numerical method for solving three-dimensional (3D) potential problems. In contrast to the BEM, the BNM requires only nodes on a boundary surface. In other words, elements of a geometrical structure are no longer necessary. However, the surface must be divided into a set of integration cells to evaluate surface integrals such as influence coefficients. In this perspective, the BNM partially retains the concept of boundary elements.

The purpose of this study is to formulate a 3D BNM that does not use any integration cells. To this end, a surface boundary is represented in terms of an implicit function [2], and the 3D local coordinates are used to evaluate surface integrals. Throughout this study, this method is called the eXtended boundary-node method (X-BNM).

2. Boundary Integral Equation

As a typical potential problem, we consider a 3D Laplace problem,

$$\Delta u = 0 \text{ in } V, \tag{1}$$

$$u = \bar{u} \text{ on } S_{\mathrm{D}}, \tag{2}$$

$$q = \bar{q} \text{ on } S_{\mathrm{N}}, \tag{3}$$

where V is a region bounded by a simple closed surface ∂V that consists of both S_{D} and S_{N}. Here, S_{D} and S_{N} satisfy $S_{\mathrm{D}} \cup S_{\mathrm{N}} = \partial V$ and $S_{\mathrm{D}} \cap S_{\mathrm{N}} = \phi$. In addition, $\bar{u}$ and $\bar{q} \equiv \partial\bar{u}/\partial n$ are known functions on S_{D} and S_{N}, respectively, and $\boldsymbol{n}$ is an outward unit normal on ∂V.

By means of Gauss' divergence theorem, the last form of the boundary integral equation can be expressed as

$$\oint_{\partial \mathrm{V}} w^*(\boldsymbol{x},\boldsymbol{y}) q(\boldsymbol{x})\, \mathrm{d}S(\boldsymbol{x}) - \oint_{\partial \mathrm{V}} \frac{\partial w^*}{\partial n}(\boldsymbol{x},\boldsymbol{y}) \left[u(\boldsymbol{x}) - u(\boldsymbol{y})\right] \mathrm{d}S(\boldsymbol{x}) = 0, \tag{4}$$

where $w^*(\boldsymbol{x},\boldsymbol{y}) \equiv (4\pi|\boldsymbol{x}-\boldsymbol{y}|)^{-1}$, and $\partial w^*(\boldsymbol{x},\boldsymbol{y})/\partial n = \boldsymbol{n}\cdot\nabla w^*$.

If $\boldsymbol{x} \in \partial V$, we assume that $u(\boldsymbol{x})$ and $q(\boldsymbol{x})$ are expressed as

$$u(\boldsymbol{x}) = \sum_{j=1}^{N} \phi_j(\boldsymbol{x})\hat{u}_j, \quad q(\boldsymbol{x}) = \sum_{j=1}^{N} \phi_j(\boldsymbol{x})\hat{q}_j, \tag{5}$$

where $\hat{u}_j$ and $\hat{q}_j$ are unknown coefficients, and $\phi_1(\boldsymbol{x}), \phi_2(\boldsymbol{x}), \ldots, \phi_N(\boldsymbol{x})$ are shape functions related to $\boldsymbol{x}_1, \boldsymbol{x}_2, \ldots, \boldsymbol{x}_N$, respectively. Here, $\boldsymbol{x}_1, \boldsymbol{x}_2, \ldots, \boldsymbol{x}_N$ are nodes on ∂V and N is the number of boundary nodes. The shape functions are generated by means of the moving least squares (MLS) approximation [1].

Substituting both $\boldsymbol{y} = \boldsymbol{x}_i$ and Eq. (5) into Eq. (4), we obtain

$$G\hat{\boldsymbol{q}} = H\hat{\boldsymbol{u}}, \tag{6}$$

where $\hat{\boldsymbol{u}} = [\hat{u}_1, \hat{u}_2, \ldots, \hat{u}_N]^{\mathrm{T}}$, and $\hat{\boldsymbol{q}} = [\hat{q}_1, \hat{q}_2, \ldots, \hat{q}_N]^{\mathrm{T}}$. G

author's e-mail: taku@st.seikei.ac.jp

and H are influence matrices whose (i, j) elements are

$$G_{ij} \equiv \oint_{\partial V} w^*(\boldsymbol{x}, \boldsymbol{x}_i)\phi_j(\boldsymbol{x})\, \mathrm{d}S(\boldsymbol{x}), \tag{7}$$

$$H_{ij} \equiv \oint_{\partial V} \frac{\partial w^*}{\partial n}(\boldsymbol{x}, \boldsymbol{x}_i)\left[\phi_j(\boldsymbol{x}) - \phi_j(\boldsymbol{x}_i)\right]\mathrm{d}S(\boldsymbol{x}). \tag{8}$$

Note that G_{ij} and H_{ij} are called influence coefficients. By assembling Eq. (6) and the discretized boundary conditions of Eqs. (2) and (3), a linear system can be obtained. By solving this linear system, we can determine $\hat{\boldsymbol{u}}$ and $\hat{\boldsymbol{q}}$. Finally, the distributions of u and q on ∂V are determined by Eq. (5).

3. Shape Functions

In the X-BNM, the shape functions $\phi_j(\boldsymbol{x})$ are generated by means of the MLS approximation. We employ a polynomial of degree $m = 1$ in the MLS approximation. Namely, the shape functions $\phi_j(\boldsymbol{x})$ are expressed as

$$\phi_j(\boldsymbol{x}) = w(|\boldsymbol{x} - \boldsymbol{x}_j|/R)\Big/\sum_i w(|\boldsymbol{x} - \boldsymbol{x}_i|/R), \tag{9}$$

where $w(\rho)$ is a weight function, and R is the radius of the support of the shape function. In the X-BNM, the following weight function is employed.

$$w(\rho) = H(1-\rho)(1 - 6\rho^2 + 8\rho^3 - 3\rho^4). \tag{10}$$

Here, $H(\rho)$ is the Heaviside function:

$$H(\rho) \equiv \begin{cases} 1 & (\rho > 0), \\ 0 & (\rho < 0). \end{cases} \tag{11}$$

3.1 Integral domain of influence coefficients

Let S_j be the part of the boundary surface ∂V that is contained in a sphere of radius R and center $\boldsymbol{x}_j$. S_j denotes the radius of the support of the shape function $\phi_j(\boldsymbol{x})$. Therefore Eqs. (7) and (8) can be expressed as

$$G_{ij} \equiv \int_{S_j} w^*(\boldsymbol{x}, \boldsymbol{x}_i)\phi_j(\boldsymbol{x})\, \mathrm{d}S(\boldsymbol{x}), \tag{12}$$

$$H_{ij} \equiv \int_{S_j} \frac{\partial w^*}{\partial n}(\boldsymbol{x}, \boldsymbol{x}_i)\phi_j(\boldsymbol{x})\mathrm{d}S(\boldsymbol{x}) + c(\boldsymbol{x}_i)\phi_j(\boldsymbol{x}_i), \tag{13}$$

where $c(\boldsymbol{x}_i) \equiv \Omega_i/(4\pi)$, and Ω_i is the solid angle on $\boldsymbol{x}_i$.

Note that the weight function in Eq. (10) was employed to satisfy $w'(0) = 0$, since we will need to determine

$$\nabla\phi_j(\boldsymbol{x}_i) = \frac{1}{R}\lim_{\boldsymbol{x}\to\boldsymbol{x}_i}\left\{-\frac{w(|\boldsymbol{x} - \boldsymbol{x}_j|/R)}{\left[\sum_k w(|\boldsymbol{x} - \boldsymbol{x}_k|/R)\right]^2} \times \sum_k w'(|\boldsymbol{x} - \boldsymbol{x}_k|/R)\frac{\boldsymbol{x} - \boldsymbol{x}_k}{|\boldsymbol{x} - \boldsymbol{x}_k|} + \frac{w'(|\boldsymbol{x} - \boldsymbol{x}_j|/R)}{\sum_k w(|\boldsymbol{x} - \boldsymbol{x}_k|/R)}\frac{\boldsymbol{x} - \boldsymbol{x}_j}{|\boldsymbol{x} - \boldsymbol{x}_j|}\right\}, \tag{14}$$

to evaluate Eqs. (12) and (13) if S_j contains a singularity $\boldsymbol{z}$ (see section 4.3 for more details).

4. Evaluation of Influence Coefficients Without Integration Cells

In the X-BNM, a boundary surface is assumed to be an implicit surface $f(\boldsymbol{x}) = 0$, and the shape function is assumed to have a support of radius R. Under the above assumption, the influence coefficients can be written in the form

$$I = \int_S F\, \mathrm{d}S. \tag{15}$$

Here, S denotes the part of the implicit surface Π that is contained in a sphere of radius R and center $\boldsymbol{y}$. Different coordinates are used for the numerical integration of Eq. (15), depending on whether S contains a singularity $\boldsymbol{z}$ of $F(\boldsymbol{x})$.

4.1 Evaluation method for $\boldsymbol{z} \notin S$

When S does not contain any singularity of $F(\boldsymbol{x})$, we use the 3D polar coordinates (ρ, θ, φ) whose center coincides with the sphere's center $\boldsymbol{y}$. In addition, we employ a local Cartesian coordinate system $\langle \boldsymbol{y} : \boldsymbol{e}'_x, \boldsymbol{e}'_y, \boldsymbol{e}'_z \rangle$ as illustrated in Fig. 1 a. In the system, $\boldsymbol{e}'_z$ is first defined as $\boldsymbol{e}'_z \equiv \nabla f(\boldsymbol{y})/|\nabla f(\boldsymbol{y})|$. After that, $\boldsymbol{e}'_x$ is generated by Schmidt orthogonalization. Finally, $\boldsymbol{e}'_y$ is defined as $\boldsymbol{e}'_y \equiv \boldsymbol{e}'_z \times \boldsymbol{e}'_x$. By using the system, arbitrary points $\boldsymbol{x}$ are expressed as follows:

$$\begin{aligned}\boldsymbol{x} &= \boldsymbol{y} + \rho(\sin\theta\cos\varphi\, \boldsymbol{e}'_x + \sin\theta\sin\varphi\, \boldsymbol{e}'_y + \cos\theta\, \boldsymbol{e}'_z) \\ &\equiv \boldsymbol{g}(\rho, \theta, \varphi).\end{aligned} \tag{16}$$

Note that, on S, θ is a function of ρ and φ, i.e., $\theta = \theta(\rho, \varphi)$ by means of the implicit function theorem. Therefore the vector equation of S is given by $\boldsymbol{x} = \boldsymbol{g}(\rho, \theta(\rho, \varphi), \varphi)$ $(0 \le \rho \le R, 0 \le \varphi < 2\pi)$. By means of this equation, the integration in Eq. (15) can be evaluated by

$$\begin{aligned} I &= \int_0^{2\pi}\mathrm{d}\varphi\int_0^R \mathrm{d}\rho F(\boldsymbol{g}(\rho, \theta(\rho, \varphi), \varphi))\left|\frac{\partial \boldsymbol{x}}{\partial\rho} \times \frac{\partial \boldsymbol{x}}{\partial\varphi}\right| \\ &= \int_0^{2\pi}\mathrm{d}\varphi\int_0^R \mathrm{d}\rho G(\rho, \varphi), \end{aligned} \tag{17}$$

where

$$\begin{aligned} G(\rho, \varphi) \equiv{}& \rho F(\boldsymbol{g}(\rho, \theta(\rho, \varphi), \varphi)) \\ &\times \left\{\left[(\theta_\rho\, \rho)^2 + 1\right]\sin^2\theta + (\theta_\varphi)^2\right\}^{1/2}. \end{aligned} \tag{18}$$

Note that $\theta(\rho, \varphi)$ is numerically determined by solving the

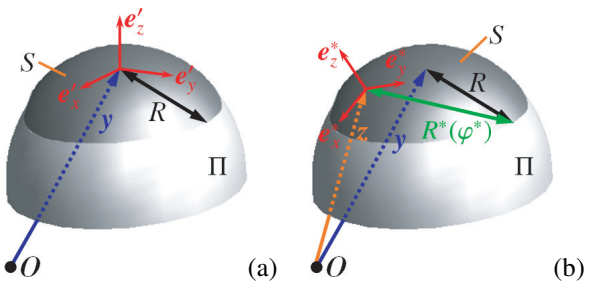

Fig. 1 Local Cartesian coordinate systems. (a) S does not contain any singularity of $F(\boldsymbol{x})$. (b) S contains a singularity $\boldsymbol{z}$ of $F(\boldsymbol{x})$.

following nonlinear equation using the Newton method.

$$f(\boldsymbol{g}(\rho,\theta,\varphi)) = 0. \tag{19}$$

4.2 Evaluation method for $z \in S$

When S contains z, a slightly different coordinate system is employed. We use the 3D polar coordinates $(\rho^*,\theta^*,\varphi^*)$ whose center is z. In addition, we employ a local Cartesian coordinate system $\langle z : \boldsymbol{e}^*_x, \boldsymbol{e}^*_y, \boldsymbol{e}^*_z\rangle$ as illustrated in Fig. 1 b. Here, $\boldsymbol{e}^*_x, \boldsymbol{e}^*_y, \boldsymbol{e}^*_z$ are defined in the same manner as $\boldsymbol{e}'_x, \boldsymbol{e}'_y, \boldsymbol{e}'_z$. By using the system, arbitrary points $\boldsymbol{x}$ are similarly expressed as in Eq. (16), that is, $\boldsymbol{x} = \boldsymbol{g}^*(\rho^*,\theta^*,\varphi^*)$. Therefore the vector equation is given by $\boldsymbol{x} = \boldsymbol{g}(\rho^*,\theta^*(\rho^*,\varphi^*),\varphi^*)$ $(0 \le \rho^* \le R^*(\varphi^*), 0 \le \varphi^* < 2\pi)$. By means of this equation, the integration in Eq. (15) can be evaluated by

$$I = \int_0^{2\pi} \mathrm{d}\varphi^* \int_0^{R^*(\varphi^*)} \mathrm{d}\rho^* G^*(\rho^*,\varphi^*), \tag{20}$$

where $G^*(\rho^*,\varphi^*)$ is defined in the same manner as in Eq. (18). Incidentally, the equation $\rho^* = R^*(\varphi^*)$ for the edge of S is determined by solving the following nonlinear systems:

$$\sigma^*_1(\rho^*,\theta^*) \equiv f(\boldsymbol{g}(\rho^*,\theta^*,\varphi^*)) = 0, \tag{21}$$

$$\sigma^*_2(\rho^*,\theta^*) \equiv |\boldsymbol{g}(\rho^*,\theta^*,\varphi^*) - \boldsymbol{y}|^2 - R^2 = 0. \tag{22}$$

Here, we employ the Newton method to solve the nonlinear systems. Note that solutions (ρ^*,θ^*) of the nonlinear systems may not converge to the appropriate ranges, which are $0 \le \rho^* \le 2R$ and $0 \le \theta^* \le \pi$. In this case, the Newton method is restarted with other initial solutions until solutions (ρ^*,θ^*) converge to $0 \le \rho^* \le 2R$ and $0 \le \theta^* \le \pi$.

4.3 Concrete form of influence coefficients

When S contains z, the integrands of the influence coefficients, Eqs. (12) and (13), are divided into terms for accurate evaluation. To divide the integrands, we use the Taylor expansion. Namely, the shape function $\phi_j(\boldsymbol{x})$ is expanded around $\boldsymbol{x}_i$ as follows:

$$\phi_j(\boldsymbol{x}) = \phi_j(\boldsymbol{x}_i) + \nabla\phi_j(\boldsymbol{x}_i)\cdot(\boldsymbol{x}-\boldsymbol{x}_i) + O(|\boldsymbol{x}-\boldsymbol{x}_i|^2). \tag{23}$$

Substituting Eq. (23) into Eqs. (12) and (13), we obtain the following divided form of influence coefficients:

$$G_{ij} = G^{\mathrm{R}}_{ij} + G^{\mathrm{D}}_{ij} + G^{\mathrm{S}}_{ij}, \tag{24}$$

$$H_{ij} = H^{\mathrm{R}}_{ij} + H^{\mathrm{D}}_{ij} + H^{\mathrm{S}}_{ij} + c(\boldsymbol{x}_i)\phi_j(\boldsymbol{x}_i), \tag{25}$$

where

$$G^{\mathrm{R}}_{ij} \equiv \int_{s_j} w^*(\boldsymbol{x},\boldsymbol{x}_i)\Big[\phi_j(\boldsymbol{x}) - \phi_j(\boldsymbol{x}_i) - \nabla\phi_j(\boldsymbol{x}_i)\cdot(\boldsymbol{x}-\boldsymbol{x}_i)\Big]\mathrm{d}S(\boldsymbol{x}), \tag{26}$$

$$G^{\mathrm{D}}_{ij} \equiv \nabla\phi_j(\boldsymbol{x}_i)\cdot\int_{s_j} w^*(\boldsymbol{x},\boldsymbol{x}_i)(\boldsymbol{x}-\boldsymbol{x}_i)\,\mathrm{d}S(\boldsymbol{x}), \tag{27}$$

$$G^{\mathrm{S}}_{ij} \equiv \phi_j(\boldsymbol{x}_i)\int_{s_j} w^*(\boldsymbol{x},\boldsymbol{x}_i)\,\mathrm{d}S(\boldsymbol{x}), \tag{28}$$

$$H^{\mathrm{R}}_{ij} \equiv \int_{s_j} \frac{\partial w^*}{\partial n}(\boldsymbol{x},\boldsymbol{x}_i)\Big[\phi_j(\boldsymbol{x}) - \phi_j(\boldsymbol{x}_i) - \nabla\phi_j(\boldsymbol{x}_i)\cdot(\boldsymbol{x}-\boldsymbol{x}_i)\Big]\mathrm{d}S(\boldsymbol{x}), \tag{29}$$

$$H^{\mathrm{D}}_{ij} \equiv \nabla\phi_j(\boldsymbol{x}_i)\cdot\int_{s_j} \frac{\partial w^*}{\partial n}(\boldsymbol{x},\boldsymbol{x}_i)(\boldsymbol{x}-\boldsymbol{x}_i)\,\mathrm{d}S(\boldsymbol{x}), \tag{30}$$

$$H^{\mathrm{S}}_{ij} \equiv \phi_j(\boldsymbol{x}_i)\int_{s_j} \frac{\partial w^*}{\partial n}(\boldsymbol{x},\boldsymbol{x}_i)\,\mathrm{d}S(\boldsymbol{x}). \tag{31}$$

Here, the super-scripts "R", "D" and "S" indicate regular, discontinuous, and singular terms, respectively. The orders of integrands of these terms are $O(\rho^*)$, $O(1)$, and $O(1/\rho^*)$, respectively, if $\rho^*(\equiv|\boldsymbol{x}-\boldsymbol{x}_i|) \ll 1$. Therefore G^{R}_{ij} and H^{R}_{ij} are evaluated by Eq. (17), since these terms no longer have any singularity. In addition, G^{D}_{ij}, H^{D}_{ij}, G^{S}_{ij}, and H^{S}_{ij} are evaluated by (20), since a singularity remains in these terms.

5. Numerical Experiments

In this section, the performance of the X-BNM is compared with that of the BEM. To this end, both methods are applied to a simple Laplace problem. The boundary ∂V is assumed to be a sphere of radius 2 whose center coincides with the origin. Throughout these numerical experiments, a known function $\bar{u}$ is given as follows: $\bar{u} = z(\sin x\cosh y + \cos x\sinh y)$. In addition, the Dirichlet condition is assumed on the boundary nodes $\boldsymbol{x}_k$ that have $z_k \ge 0$, and the Neumann condition is assumed on other boundary nodes. For the shape functions $\phi_i(\boldsymbol{x})$, radii are set so that at least four nodes are contained inside each radius. Note that all the shape functions have the same length of radius in these numerical experiments.

For the BEM, the boundary ∂V is divided into a set of triangles for discretization. Figure 2 shows the result of the discretization for 1004 boundary nodes. The boundary nodes are at the same positions as the vertices of the triangles. For the X-BNM, the same boundary nodes are employed. The linear systems of both methods are solved by means of the Gaussian elimination method. To numerically integrate Eqs. (17) and (20), the trapezoid formula and Gauss-Legendre quadrature are applied to the φ and ρ directions, respectively.

Computations were performed on a computer equipped with dual 2.8 GHz Quad-Core Intel Xeon

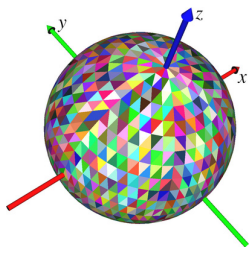

Fig. 2 Result of discretization for the BEM with 1004 boundary nodes. Colors of triangles are assigned randomly to distinguish each triangle easily.

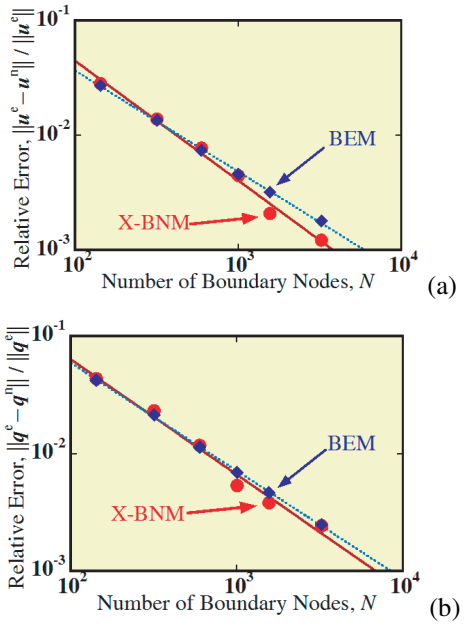

Fig. 3 (a) Relationship between the number N of boundary nodes and the relative error ε_u. (b) Relationship between the number N of boundary nodes and the relative error ε_q.

processors, 24 GB RAM, Mac OS X ver. 10.5.8, and g++ ver. 4.4.0. Note that we used only a single core of the computer for the computations.

First we investigate the accuracy of both methods. The relative errors for u and q are defined as

$$\varepsilon_u = \frac{\|\boldsymbol{u}^{\mathrm{e}} - \boldsymbol{u}^{\mathrm{n}}\|_2}{\|\boldsymbol{u}^{\mathrm{e}}\|_2}, \text{ and } \varepsilon_q = \frac{\|\boldsymbol{q}^{\mathrm{e}} - \boldsymbol{q}^{\mathrm{n}}\|_2}{\|\boldsymbol{q}^{\mathrm{e}}\|_2}, \tag{32}$$

respectively, where $\boldsymbol{u}^{\mathrm{e}} = [u_1^{\mathrm{e}}, u_2^{\mathrm{e}}, \ldots, u_N^{\mathrm{e}}]^{\mathrm{T}}$, $\boldsymbol{u}^{\mathrm{n}} = [u_1^{\mathrm{n}}, u_2^{\mathrm{n}}, \ldots, u_N^{\mathrm{n}}]^{\mathrm{T}}$, $\boldsymbol{q}^{\mathrm{e}} = [q_1^{\mathrm{e}}, q_2^{\mathrm{e}}, \ldots, q_N^{\mathrm{e}}]^{\mathrm{T}}$, and $\boldsymbol{q}^{\mathrm{n}} = [q_1^{\mathrm{n}}, q_2^{\mathrm{n}}, \ldots, q_N^{\mathrm{n}}]^{\mathrm{T}}$. Here, the super-scripts "e" and "n" indicate exact and numerical solutions, respectively. Both relative errors are calculated as a function of N and are shown in Figs. 3a and 3b, respectively. In each figure, power regression curves are fitted to the relative errors. Note that the curves are illustrated as lines in Figs. 3a and 3b, since both figures are logarithmic graphs. In Fig. 3a, the slope of the line for the X-BNM is about -1.0, and that for the BEM is about -0.88. In Fig. 3b, the slope of the line for the X-BNM is about -0.98, and that for the BEM is about -0.92. From Figs. 3a and 3b, we see that there is no obvious difference between the relative errors of the methods. That is, for the Laplace problem, the accuracy of the X-BNM is almost the same as that of the BEM.

Next, we investigate the dependence of the computational time on the number N of boundary nodes for the X-BNM and the BEM, as shown in Fig. 4. The computational times required for the X-BNM are larger than those for the BEM. Note that the size of the coefficient matrix of the linear system for the X-BNM is $2N \times 2N$, and that for the BEM is $N \times N$. Hence, the computational time of the X-BNM may be at least eight times as large as that of the BEM, since the order of the Gaussian elimination method

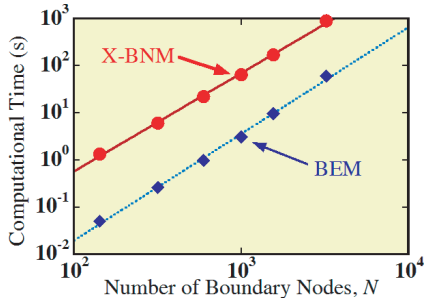

Fig. 4 Dependence of computational time on the number N of boundary nodes.

is $O(N^3/3)$. In order to evaluate Eqs. (17) and (20), the X-BNM also requires some additional computations, such as solving the nonlinear equation in Eq. (19) and solving the nonlinear systems of Eqs. (21) and (22).

As a result, although the computational costs of the X-BNM are larger than those of the BEM, the X-BNM enables the evaluation of surface integrals without any integration cells. In addition, the accuracy of the X-BNM is almost equal to that of the BEM.

6. Conclusion

A BNM without any integration cells has been formulated. In this formulation, an implicit surface is assumed as a surface boundary, and the 3D local coordinates are used to evaluate surface integrals. The Laplace problem is chosen as a typical potential problem, and the performance of the X-BNM is investigated numerically. Conclusions obtained in the present study are summarized as follows:

1. The computational costs of the X-BNM are larger than those of the BEM.
2. The X-BNM enables the evaluation of surface integrals without any integration cells.
3. For the Laplace problem, the accuracy of the X-BNM is almost the same as that of the BEM.

In a future investigation, the Krylov subspace methods will be employed to solve the linear systems in order to decrease the computational costs. Furthermore, solvers for the nonlinear systems in Eqs. (21) and (22) will be investigated for fast evaluation of numerical integrations. In addition, a higher degree of polynomial for the MLS approximation will be investigated to obtain a better solution.

Acknowledgment

This work was supported by KAKENHI (No. 20700098) and by the NIFS Collaboration Research Program (NIFS09KDBN003).

[1] M. K. Chati and S. Mukherjee, Int. J. Numer. Methods Eng. **47**, 1523 (2000).
[2] Y. Ohtake, A. Belyaev, M. Alexa, G. Turk and H.-P. Seidel, ACM Trans. Graph. **22**, 463 (2003).